On the Residual Errors Mitigation in Single-Frequency Code-Based Real-Time PPP

Izadora A. Ramos[1,†], Vinícius M. G. B. Cavalcanti[2,†], Felipe O. Silva[1,*,†] and Danilo A. de Lima[1]

[1]*Federal University of Lavras, Trevo Rotatório Professor Edmir Sá Santos, 37203-202, Lavras, Brazil*
[2]*Fluminense Federal Institute, Rua Izaura Pantoja, 167, Nova Cidade, 24804-162, Itaboraí, Brazil*

Abstract

Real-Time Precise Point Positioning (RT-PPP) aims at improving positioning accuracy by correcting Common Mode Errors (CMEs) present in Global Navigation Satelite System (GNSS) observables. This is done by means of products made available, in real-time, by specialized agencies, such as the International GNSS Service (IGS) and the Faculty of Astronomical and Geophysical Sciences (FCAG) of the Argentine University of La Plata (UNLP). Nevertheless, after applying the RT-PPP corrections, residual errors remain in the GNSS observables, which need to be addressed if one aims to further improve positioning accuracy. Among the latter, stands out: (a) the tropospheric error, which is a CME for which no RT-PPP products are currently provided; and (b) the multipath error, which is a Non-Common Mode Error (NCME) whose effect is associated with the reception of multiple GNSS signals reflected from the surrounding environment. In this work, we propose to estimate the residual multipath errors as 1st-order Gauss-Markov (GM) processes, which are augmented to the Extended Kalman Filter (EFK) state vector, after having their correlation times and driven noise Power Spectral Densities (PSDs) suitably identified. For the tropospheric error, we estimate (and compensate) the latter via the University of New Brunswick 3 (UNB3) empirical model, and we augment the EKF for one additional state, to account for the residual zenith wet tropospheric delay, which is modeled according to Niell's mapping function. The very aim of this work is to evaluate the effectiveness of the aforementioned techniques, specifically aiming at the compliance with positioning accuracy requirements of Single-Frequency (SF) code-based GNSS receivers-equipped Connected Vehicle Applications (CVAs). As main contribution, we show that the estimation of the residual zenith wet tropospheric delay in the EKF state vector improves the position accuracy of the RT-PPP solution, particularly in the vertical channel (8% of improvement). As for the estimation of the multipath errors, however, the latter is not seen to be true (30% of impairment). Results from a dynamic test supports the outlined verifications.

Keywords

GNSS, RT-PPP, EKF, Multipath, Troposphere

1. Introduction

Global Navigation Satellite Systems (GNSSs) positioning is based on the transmission of signals from orbiting satellites, which provide us with three types of measurements: pseudoranges, Doppler shifts, and carrier phases. GNSS signals are affected by several sources of errors that deteriorate the position solution. Pseudorange measurements (the main GNSS observable employed in mass market applications and, hence, the one we focus on throughout this work are primarily corrupted by nine types of errors [1, 2], which can be classified into two categories [3]:

- *Common Mode Errors (CMEs)*, which are spatially and temporally correlated errors, i.e., they are experienced similarly by all receivers in the same vicinity over short time intervals. They comprise the ephemeris error, satellite clock bias, satellite hardware bias, ionospheric and tropospheric delays;

- *Non-Common Mode Errors (NCMEs)* are different for each receiver (even when separated by short distances), being comprised of receiver clock bias, receiver hardware bias, multipath error, and receiver tracking noise.

Real-Time Precise Point Positioning (RT-PPP) is a state-of-the-art technique that provides compensation for (most of) the CMEs, via products that are made available, over the internet and in real-time, by specialized agencies. The International GNSS Service (IGS) currently provides RT-PPP corrections with global coverage for satellite orbits; clock and hardware biases; and ionospheric delays. In parallel to IGS, regional agencies have recently succeeded in establishing correction services to serve their local users better. For example, Silva, Hu, and Farrell [4] showed that the ionospheric products broadcasted by the Faculty of Astronomical and Geophysical Sciences (FCAG) of the Argentine University of La Plata (UNLP) [5] attained superior performance w.r.t. the real-time ionospheric corrections provided by the IGS, for Connected Vehicle Applications (CVAs) in Brazilian territory (focus of this work).

To the best of the authors' knowledge, the tropospheric error is the sole CME for which no RT-PPP products are currently provided by any specialized agency, even though they are foreseen in the third stage of deployment of the IGS Real-Time Service (RTS) [6]. As conceptualized by Groves [7], the troposphere is a nondispersive medium, so all GNSS signals are delayed equally and there is no code−carrier divergence. On average, about 90% of the delay is due to the dry gases in the atmosphere and is relatively stable. The remaining delay relates to water vapor and varies considerably. The total tropospheric delay at the zenith is about 2.5 m and varies by about ±10% with the climate and weather.

As a solution for the current unavailability of RT-PPP tropospheric products, users have resorted to the deployment of empirical models. In Brazilian territory, for instance, Oliveira *et al.* [8] showed that the University of New Brunswick 3 (UNB3) is the model that performs best in terms of positioning accuracy. UNB3 is a neutral atmosphere-based tropospheric delay model that employs predictions of meteorological parameter values for a given location, i.e., it depends on the latitude and altitude of the user and day of the year. These parameters are used to calculate hydrostatic (dry) and non-hydrostatic (wet) zenith delays using Saastamoinen models [9]. Slant delays (and/or lag rates) are then determined using Niell mapping functions (or mapping function rates in the case of lag rates) [10].

As analyzed by Conley *et al.* [11], residual errors of around 0.2 m are expected to exist when using UNB3 model, which relates, mostly, to the associated residual wet delays. In this regard, best performance can be obtained by using current temperature, pressure, and humidity data. The incorporation of meteorological sensors in most navigation applications, however, is not practical. As analyzed by Groves [7], for high-precision applications, the residual wet troposphere propagation errors may be calibrated as part of the navigation solution. This exploits the high degree of correlation between the errors on signals from different satellites and may improve the positioning accuracy by a few centimeters.

In addition to the tropospheric residual error, the NCMEs are also not compensated for when deploying RT-PPP. While the tracking noise is usually considered to be sufficiently white, and the receiver clock and hardware biases can be easily estimated or compensated for by differencing the pseudoranges across satellites, the multipath error stands out as the major source of residual NCMEs corrupting the observables. The multipath is the phenomenon whereby the signal from a satellite arrives at the receiver via multiple paths due to reflection and diffraction. These non-direct path signals distort the received signal and cause errors both in code (pseudorange) and phase measurements, which might be at the meter- and centimeter-level, respectively [12].

Several studies have been conducted to mitigate multipath errors. Without loss of generality, the techniques may be categorized as depending on the: (a) antenna placement; (b) antenna type; (c) receiver type; and (d) measurement post-processing, which deals with multipath-contaminated measurements [13]. There are numerous applications in which multipath is unavoidable despite the best attempts at an optimum choice of antenna placement/design, and receiver architecture.

In this work, hence, we focus on evaluating the performance of filtering-based techniques for mitigating the residual wet tropospheric error and the multipath error that remains after SF code-based RT-PPP deployment. From the estimation standpoint, we tackle the problem by adding one state to the

associated Extended Kalman Filter (EFK), to account for the residual wet part of the tropospheric error at zenith (mapped w.r.t. to the visible satellites by means of Niell obliquity functions [10]). As for the multipath errors, we augment the EKF state vector by the same number of visible satellites, and we model the latter as a 1st-order Gauss-Markov (GM) processes (with correlation times and the driven noise Power Spectrum Densities (PSDs) previously and meticulously identified). As main contribution of this work, we show, via a dynamic experimental test, that the EKF estimation of the residual zenith wet tropospheric error, in fact, improves the accuracy of the RT-PPP solution, particularly in the vertical channel. The estimation of the multipath errors, in turn, does not seem to bring additional benefits.

The remainder of this work is organized as follows: Section 2 introduces the notation, GNSS background for SF code-based RT-PPP estimation, and the associated EKF modeling for the residual tropospheric and multipath errors. Section 3 describes the procedure used to suitably identify the parameters that model the residual multipath errors as 1st-order GM processes. Section 4 describes the experimental data acquisition and discusses the outcomes in terms of positioning performance. Section 5, lastly, summarizes the paper and presents final thoughts.

2. GNSS Background

The raw (subscript R) pseudorange measurement between the user antenna a and satellite s, taking into account the errors cited in Section 1, can be modeled as [14]:

$$\rho_{a,R}^s = \left| \mathbf{C}_e^I \, \mathbf{r}_{es}^e - \mathbf{r}_{ea}^e \right| + \delta\rho_E^s - \delta\rho_c^s + \delta\rho_b^s + \delta\rho_{I,a}^s + \delta\rho_{T,a}^s + \delta\rho_c^a + \delta\rho_b^a + \delta\rho_{M,a}^s + w_{\rho,a}^s, \quad (1)$$

where $\mathbf{C}_e^I$ is the Direct Cosine Matrix (DCM) compensating for the Earth-Centered-Earth-Fixed (ECEF) frame rotation during signal propagation (for details, please refer to section 2.4.1 from [12]); $\mathbf{r}_{es}^e$ is the ECEF satellite position at time of signal transmission; and $\mathbf{r}_{ea}^e$ is the ECEF user position at time of signal reception. The second row in (1) represents the pseudorange CMEs ($\delta\rho_E^s$ is the ephemeris error, $\delta\rho_c^s$ and $\delta\rho_b^s$ are the satellite clock and hardware code biases, respectively, $\delta\rho_{I,a}^s$ is the ionospheric delay, and $\delta\rho_{T,a}^s$ is the tropospheric delay); and the third row, the NCMEs ($\delta\rho_c^a$ and $\delta\rho_b^a$ represent the receiver clock and hardware code biases, respectively, $\delta\rho_{M,a}^s$ is the multipath error, and $w_{\rho,a}^s$ is the receiver tracking noise).

As discussed in Section 1, the tropospheric delay, $\delta\rho_{T,a}^s$, can be divided into two components: (a) the dry part, accounting for approximately 90% of the total delay, which can be more accurately modeled by means of empirical models; and (b) the wet part, which is more complex to model, due to its variation with climate and weather. According to Niell [10], one has:

$$\delta\rho_{T,a}^s = m_d^s \tau_d^z + m_w^s \tau_w^z \quad (2)$$

where τ_d^z and τ_w^z are the zenith delays for the dry and wet tropospheric components, respectively, and m_d^s and m_w^s are the dry and wet mapping functions, also respectively, which can be defined as [15]:

$$m_i^s = \cfrac{\cfrac{1}{1 + \cfrac{a}{1 + \cfrac{b}{1 + c}}}}{\sin(\epsilon) + \cfrac{a}{\sin(\epsilon) + \cfrac{b}{\sin(\epsilon) + c}}} \quad (3)$$

where $i \in \{d, w\}$, the coefficients a, b and c are constants defined in [10], which are functions of the latitude, and ϵ is the satellite elevation angle.

Following the deployment of SF code-based RT-PPP, most of the CMEs depicted in (1) may be considered to have been accurately compensated for. The ephemeris error, satellite clock and hardware code biases, for instance, may be corrected using State Space Representation (SSR) products from

the IGS RTS. The ionospheric error, in turn, particularly for Latin America users (with extension to the Caribbean and the Antarctica peninsula), may be mitigated via the deployment of the Regional Ionospheric Maps (RIMs) from the UNLP FCAG, and the dry (and most of the wet) components of the tropospheric error, lastly, by the application of the empirical UNB3 model. Details on the applicable models for SF code-based RT-PPP deployment are not given in this work. The interested reader is invited to refer to [4, 16, 17].

After the deployment of such SF code-based RT-PPP compensations (subscript C), (1) can be re-written as:

$$\rho_{a,C}^s = \left| \mathbf{C}_e^I \, \mathbf{r}_{es}^e - \mathbf{r}_{ea}^e \right| + m_w^s \delta\tau_w^z + \delta\rho_c^a + \delta\rho_b^a + \delta\rho_{M,a}^s + w_{\rho,a}^s, \tag{4}$$

where $\delta\tau_w^z$ is the residual wet tropospheric delay at zenith.

Even though the lumped effect of the receiver clock and hardware code biases in (4) can easily estimated (as these error terms corrupt equally every observation measurement from the visible satellites to the receiver), it is usually more advised to remove the latter by means of forming pseudorange observations differenced across satellites, i.e., Single-Differenced (SD) observations:

$$\nabla\rho_{a,C}^{ps} = \rho_{a,C}^s - \rho_{a,C}^p. \tag{5}$$

where p is the pivot satellite (usually the one with highest elevation angle [7]).

A suitable model for (5) is then:

$$\nabla\rho_{a,C}^{ps} = \left| \mathbf{C}_e^I \, \mathbf{r}_{es}^e - \mathbf{r}_{ea}^e \right| + \left| \mathbf{C}_e^I \, \mathbf{r}_{ep}^e - \mathbf{r}_{ea}^e \right| + (m_w^s - m_w^p)\delta\tau_w^z + \nabla\delta\rho_{M,a}^{ps} + \nabla w_{\rho,a}^{ps}, \tag{6}$$

where $\nabla\delta\rho_{M,a}^{ps}$ and $\nabla w_{\rho,a}^{ps}$ are the SD multipath error and tracking noise, respectively.

The parameter of interest in the estimation problem of (6) is the user position, whose functional relationship to the SD pseudorange measurement is nonlinear. Examples of methods used to estimate the latter are the Weighted Iterated Least Squares (WILS) and the Extended Kalman Filter (EKF). When a filtered GNSS approach is implemented (focus of this work), the Kalman filter state vector definition may vary according to the desired application. In general, the position and velocity vectors are always estimated. Based on the measurement model of (6), and assuming that the residual zenith wet tropospheric delay and the SD multipath errors are observable/estimable, the following state vector can be proposed:

$$\mathbf{x}^e = [(\mathbf{r}_{ea}^e)^T, (\mathbf{v}_{ea}^e)^T, \delta\tau_w^z, \nabla\delta\rho_{M,a}^{p1}, ..., \nabla\delta\rho_{M,a}^{pm}]^T \in \mathbb{R}^{m+7} \tag{7}$$

where $\mathbf{v}_{ea}^e$ is the ECEF-referenced receiver velocity and m is the number of visible satellites (not accounting for satellite p).

The state variables in (7) can be propagated in time, during the prediction step of the EKF, via the following dynamic models [7]:

$$\dot{\mathbf{r}}_{ea}^e = \mathbf{v}_{ea}^e \tag{8}$$

$$\dot{\mathbf{v}}_{ea}^e = \mathbf{w}_a \tag{9}$$

$$\dot{\delta\tau}_w^z = w_\tau \tag{10}$$

$$\nabla\delta\dot{\rho}_{M,a}^{ps} = -\beta_M^{ps}\nabla\delta\rho_{M,a}^{ps} + w_M^{ps}. \tag{11}$$

where β_M is the inverse of the SD multipath error correlation time, and $\mathbf{w}_a$, w_τ and w_M are the acceleration, residual zenith wet tropospheric error, and SD multipath error driven noises, respectively, whose statistics are deemed to be sufficiently known in order to the EKF process noise density matrix to be suitably tuned (details will be discussed in Section 3).

Considering the availability of m SD pseudorange measurements, the Jacobian operator can be applied to the measurement model of (6), yielding the following measurement matrix for the update stage of the EKF:

$$H^e = \begin{bmatrix} -(\mathbf{u}_{a1}^e - \mathbf{u}_{ap}^e)^T & 0_{1\times3} & (m_w^1 - m_w^p) & 1 & \dots & 0 \\ \vdots & \vdots & \vdots & \vdots & \ddots & \vdots \\ -(\mathbf{u}_{am}^e - \mathbf{u}_{ap}^e)^T & 0_{1\times3} & (m_w^m - m_w^p) & 0 & \dots & 1 \end{bmatrix} \tag{12}$$

where $\mathbf{u}_{as}^e$ is the ECEF-resolved line-of-sight vector from satellite s to the receiver antenna a.

As for the EKF measurement noise covariance matrix, lastly, it is expected to be correlated between the SD pseudorange measurements, and it shall be tuned based on the statistics of the SD tracking noises (generally considered to be functions of the satellite elevation angles, signal-to-noise attenuation, and/or receiver acceleration [7]).

3. Multipath Error Model Identification

To allow the SD multipath error states in (7) to be suitably accounted for in the EKF prediction model, it is of paramount importance that the parameters that model their dynamic propagation match the true ones, to the best accuracy possible. Below, we present the strategy adopted in this paper, as adapted from [18], for correctly identifying the correlation times and the driven noise Power Spectral Densities (PSDs) of the 1st-order GM processes herein proposed to model the SD multipath errors.

Following the pseudorange measurement model of (1), let us define the following model for the associate carrier-phase measurement [14, 18]:

$$\Phi_{a,R}^s = \left| \mathbf{C}_e^I \, \mathbf{r}_{es}^e - \mathbf{r}_{ea}^e \right| + \delta\rho_E^s - \delta\rho_c^s + \delta\Phi_b^s - \delta\rho_{I,a}^s + \delta\rho_{T,a}^s$$
$$+ \delta\rho_c^a + \delta\Phi_b^a + \delta\Phi_{M,a}^s + N_a^s \lambda_{ca} + \omega_{\Phi,a}^s, \quad (13)$$

where $\delta\Phi_b^s$ and $\delta\Phi_b^a$ are the satellite and receiver hardware phase biases, respectively, $\delta\Phi_{M,a}^s$ is the carrier phase multipath error, N_a^s is the integer ambiguity, λ_{ca} is the carrier wavelength, and $\omega_{\Phi,a}^s$ is the carrier phase tracking noise.

From (1) and (13), it is possible to see that the true range, ephemeris error, satellite and receiver clock biases, and the tropospheric delay are common both to the pseudorange and carrier-phase measurement models. Thus, the difference of such measurements, sometimes referred to as Code-Minus-Carrier (CMC), yields:

$$x_s = \rho_{a,R}^s - \Phi_{a,R}^s \equiv 2\delta\rho_{I,a}^s + (\delta\rho_b^s - \delta\Phi_b^s) + (\delta\rho_b^a - \delta\Phi_b^a)$$
$$+ (\delta\rho_{M,a}^s - \delta\Phi_{M,a}^s) + N_a^s \lambda_{ca} + (w_{\rho,a}^s - w_{\Phi,a}^s). \quad (14)$$

Assuming that the carrier-phase tracking noise and multipath errors are negligible compared to those of the pseudorange, and that the hardware code and phase bias differences are also negligible, (14) simplifies to:

$$x_s \approx 2\delta\rho_{I,a}^s + \delta\rho_{M,a}^s + N_a^s \lambda_{ca} + \omega_{x,a}^s, \quad (15)$$

where the term $\omega_{x,a}^s$ accounts for the pseudorange error noise plus residuals related to underlying simplifying assumptions.

If an estimate of the ionospheric error, $\delta\hat{\rho}_{I,a}^s$, is available, then we may compute:

$$y_s = x_s - 2\delta\hat{\rho}_{I,a}^s \equiv N_a^s \lambda_{ca} + \delta\rho_{M,a}^s + \omega_{y,a}^s, \quad (16)$$

where $\omega_{y,a}^s$ adds residual ionospheric error to $\omega_{x,a}^s$.

If dual-frequency carrier phase measurements are available (e.g., from frequencies f_{L1} and f_{L2} of the Global Positioning System (GPS)), it is possible to compute a relative ionospheric delay which includes the multipath, a constant integer ambiguity and residual terms (noise). In equation:

$$\delta\hat{\rho}_{I,a}^s = \left(\frac{(f_{L2})^2}{(f_{L1})^2 - (f_{L2})^2} \right) \left(\Phi_{a,R}^{s,L1} - \Phi_{a,R}^{s,L2} \right). \quad (17)$$

Therefore, a closed-form expression for the ionosphere-corrected CMC observable, y_s, can be alternatively computed as [13]:

$$y_s = \rho_{a,R}^s - \left(\frac{(f_{L1})^2 + (f_{L2})^2}{(f_{L1})^2 - (f_{L2})^2} \right) \Phi_{a,R}^{s,L1} + \left(\frac{2(f_{L2})^2}{(f_{L1})^2 - (f_{L2})^2} \right) \Phi_{a,R}^{s,L2}. \quad (18)$$

Now, assuming that the carrier tracking-loop has not experienced any cycle slips, the integer ambiguity $N_a^s \lambda_{ca}$ is constant and can be removed by subtracting the mean value of y_s, i.e. $\bar{y}_s$, from (18), as follows:

$$
\begin{aligned}
z_s &= y_s - \bar{y}_s \\
&\equiv \delta\rho_{M,a}^s + \omega_{z,a}^s,
\end{aligned}
\tag{19}
$$

which encompass the pseudorange multipath error plus the tracking noise and various residual errors neglected due to the previous analysis assumptions [18].

As it is straightforward to infer from (19), z_s unequivocally characterizes the multipath error $\delta\rho_{M,a}^s$ that corrupts the pseudorange measurement from satellite s to the receiver antenna a. Such signal, once computed for satellite p, can be subtracted from the latter to characterize the SD pseudorange multipath error $\delta\rho_{M,a}^{ps}$, i.e.,

$$
z_{ps} = z_s - z_p
\tag{20}
$$

which can be modeled as a 1st-order GM process:

$$
\dot{z}_{ps} = -\beta_z z_{ps} + \omega_z.
\tag{21}
$$

Signal z_{ps} exhibits the exponential autocorrelation property

$$
R_{z_{ps}}(\tau) = \sigma_{z_{ps}}^2 e^{-\beta_z |\tau|}.
\tag{22}
$$

where $\sigma_{z_s}^2$ is the variance of signal z_{ps}.

The correlation time $\tau_z \triangleq \beta_z^{-1}$ can be extracted from the autocorrelation function for the point when $\beta_z |\tau| = 1$ holds [19]. In practice, one shall search for an estimated correlation time $\hat{\tau}_z$, related to the minimal difference between the experimental autocorrelation function $\tilde{R}_{z_{ps}}$ and the theoretical value $R_{z_{ps}}(\tau_z)$.

$$
\hat{\tau}_z \triangleq \arg\min_{\tau \in T} \left(\tilde{R}_{z_{ps}}(\tau) - \sigma_{z_{ps}}^2 e^{-1} \right).
\tag{23}
$$

The driven noise PSD of z_{ps}, in turn, can be computed using the following relation [19]:

$$
S_{w_z} = 2\hat{\beta}_z \tilde{R}_{z_{ps}}(0).
\tag{24}
$$

Equations (23) and (24) summarize the identification procedure that is to be implemented to suitably characterize the SD pseudorange multipath errors modeled as states in (7).

4. Experimental Results

To verify the effectiveness of the filtering techniques herein proposed for mitigating the residual multipath and zenith wet tropospheric errors remaining after the SF code-based RT-PPP deployment, four different estimation combinations were considered in this work:

- SD strategy: Standard SD code-based RT-PPP estimation via EKF, with the regular 6 states;
- ZT strategy: SD code-based RT-PPP estimation via EKF, with 1 additional state to account for the zenith wet tropospheric error;
- MP strategy: SD code-based RT-PPP estimation via EKF, with m additional states to model the SD multipath errors;
- ZT+MP strategy: SD code-based RT-PPP estimation via EKF, with $m + 1$ additional states in order to account for the zenith wet tropospheric error and the SD multipath errors.

A dynamic experimental test was carried out, which aimed at validating the investigated approaches in the scope of CVAs (main focus of this work), as described in sequence.

4.1. Experimental Data Acquisition and Methodology

The dynamic test consisted of collecting L1 Coarse Acquisition (C/A) GPS observation data from an automotive-grade u-blox C102-F9R receiver and an ANN-MB-01 antenna attached to a car on July 21, 2023, in Lavras-MG, Brazil. The car was driven for a couple of minutes through the streets of a neighborhood close to the Federal University of Lavras (UFLA), executing all types of motion that are typical for urban scenarios, such as curves, accelerations, decelerations, climbs, descents, stops, etc (Figure 1). Along with the observation data, the BKG NTRIP Client (BNC) software was used to collect the SSR RT-PPP products from the IGS RTS, namely, SSRA02IGS1, which is an IGS Kalman filter combined solution that conveys satellite orbit, clock, and hardware bias corrections [20]. The UNLP FCAG RT RIM products were collected directly from its File Transfer Protocol (FTP) server in the IONEX format [21, 22]. As for the compensation of the tropospheric errors, the UNB3 empirical model was adopted. To help in obtaining a reliable ground-truth solution for the test, the GPS observation data and navigation message from a Continuous Operating Reference Station (CORS) located at Lavras (acronym MGLA), belonging to the Brazilian Network for Continuous Monitoring (RBMC) of GNSS, and distant to the car of about 1 km, were directly obtained from the Brazilian Institute of Geography and Statistics (IBGE) repository.

After the GPS data acquisition and conversion (from proprietary .UBX format to Receiver INdependent EXchange (RINEX) format version 2.11, via RTKLIB software [23]), the latter were analyzed and processed offline using specialized MATLAB algorithms developed by the authors, which employed the four aforementioned estimation strategies to compute the position solutions. The errors were calculated w.r.t. the ground-truth profile, which was obtained by processing dual-frequency double-differenced pseudorange, and integer-resolved carrier-phase observables from the same u-blox C102-F9R module
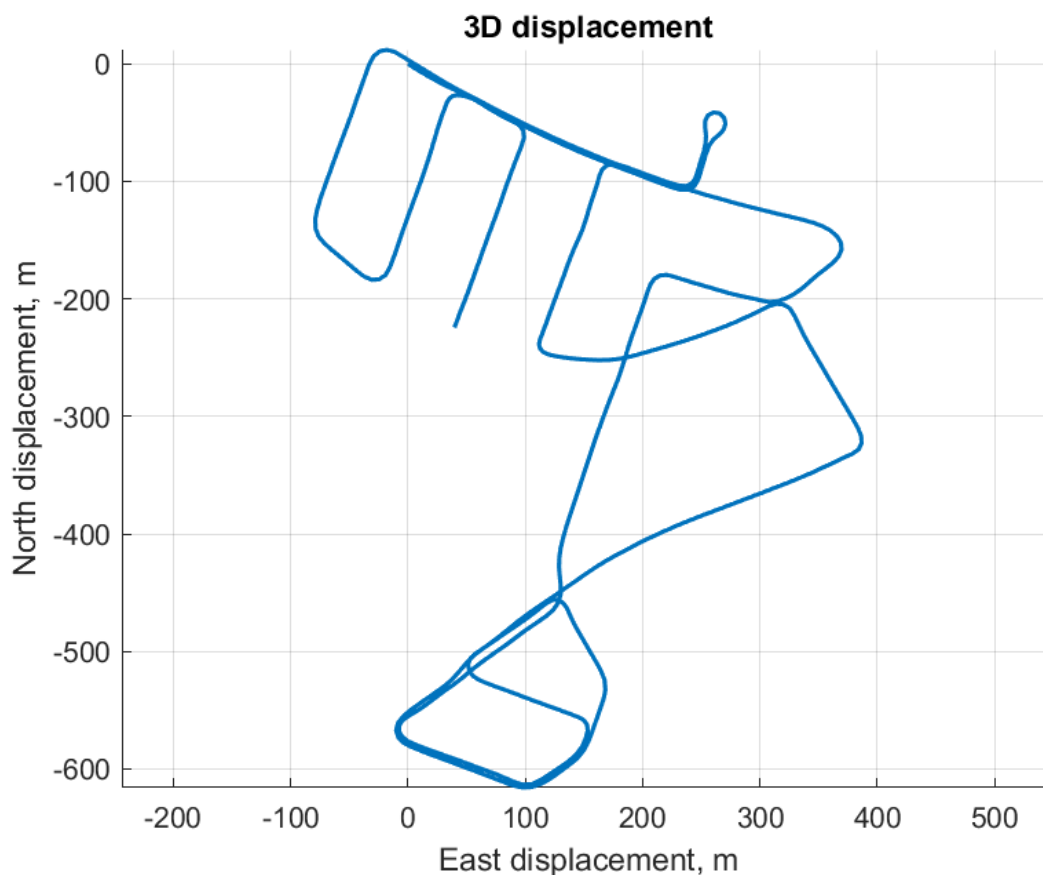
Figure 1: Ground-truth profile.

connected, via the internet, to the MGLA reference station.

To assess the effectiveness of the filtering-based estimation strategies under investigation, the horizontal, vertical, and total Cartesian position errors of the GNSS receiver antenna were established as metrics:

$$\delta r^e_{ea,H} = \sqrt{(\delta r^e_{ea,N})^2 + (\delta r^e_{ea,E})^2} \tag{25}$$

$$\delta r^e_{ea,V} = \sqrt{(\delta r^e_{ea,D})^2} \tag{26}$$

$$\delta r^e_{ea,T} = \sqrt{(\delta r^e_{ea,N})^2 + (\delta r^e_{ea,E})^2 + (\delta r^e_{ea,D})^2} \tag{27}$$

where $\delta r^e_{ea,N}$, $\delta r^e_{ea,E}$, and $\delta r^e_{ea,D}$ are the Cartesian position errors along north, east, and down directions, respectively.

As the focus of this work is on CVA applications, we also checked the ability of the estimation strategies to comply with the Society of Automotive Engineers (SAE) standard J2945 [24], which establishes maximum horizontal and vertical position errors of 1.5 m and 3.0 m, respectively, at 68% of probability (1σ).

4.2. Performance Analysis

Table 1 summarizes the results for the dynamic test in terms of mean position errors. Figures 2 to 4, in turn, show the Cumulative Distribution Functions (CDFs) for the horizontal, vertical and total channel, respectively. Tables 2 to 4, lastly, give the percentile of samples that are below some specific position error thresholds for the horizontal, vertical, and total channels, also respectively. The best results are highlighted in green and the worst in red. As can be seen, all four estimation strategies were able to comply with SAE J2945 standard position accuracy requirements. While, for the horizontal channel, the investigated strategies did not differ significantly in terms of delivered accuracy, for the vertical channel, the ZT strategy (the best performing approach) improved over the regular SD strategy in about 8%, reducing the mean vertical position error in 12 centimeters. Worthy of note is the fact that, for the vertical channel, the MP and ZT+MP strategies not only were unable to improve accuracy, as they actually increased the mean vertical position error (in 30% and 35%, respectively). As a straightforward consequence of the latter, the performance of the strategies in terms of total position error followed the same pattern of the vertical channel's.
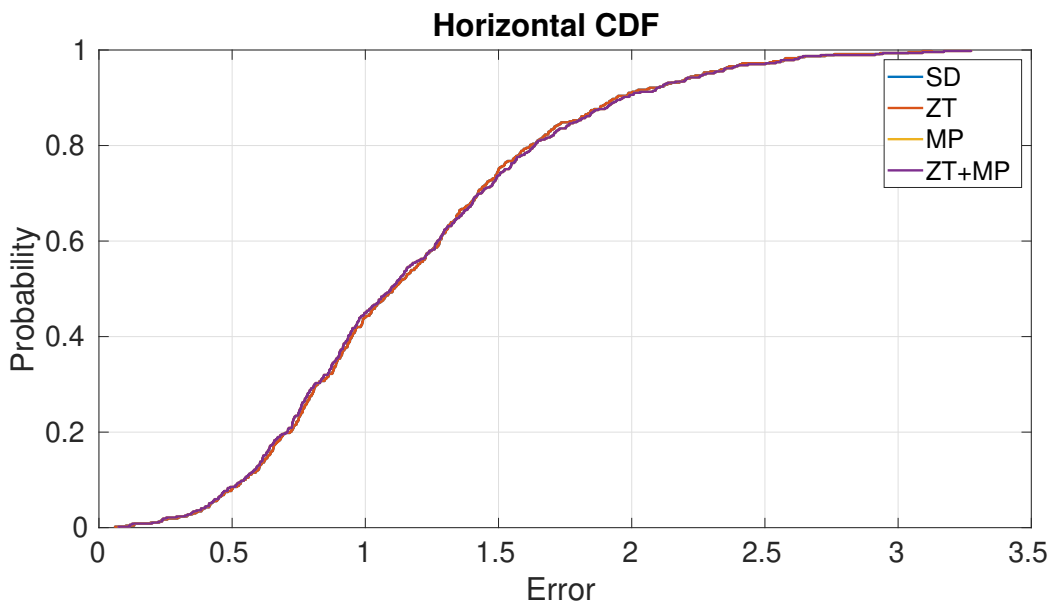
Figure 2: Horizontal Cumulative Distribution (errors are in meters).
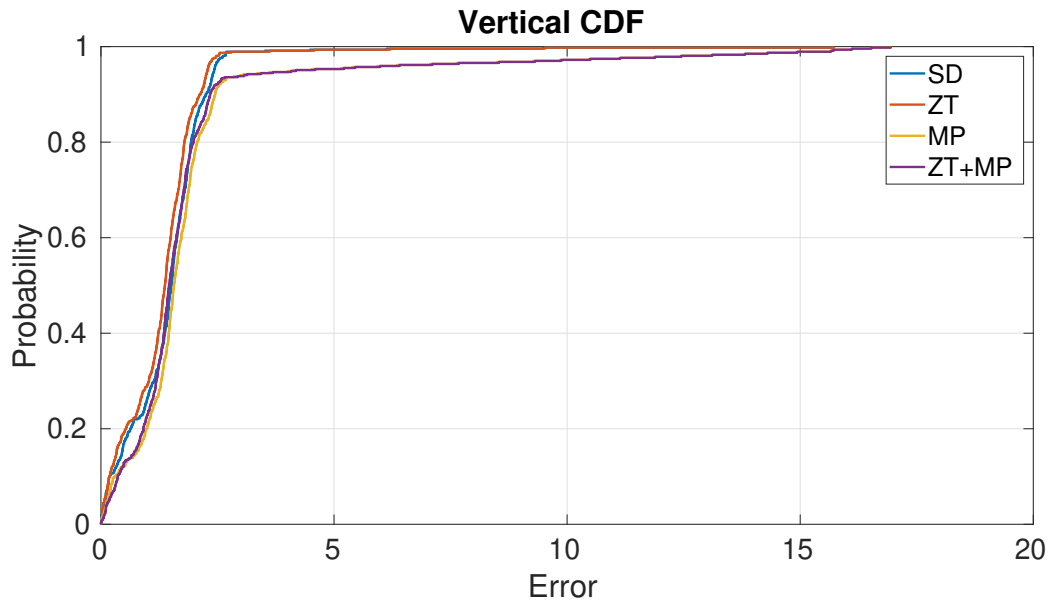
Vertical CDF

Figure 3: Vertical Cumulative Distribution (errors are in meters).
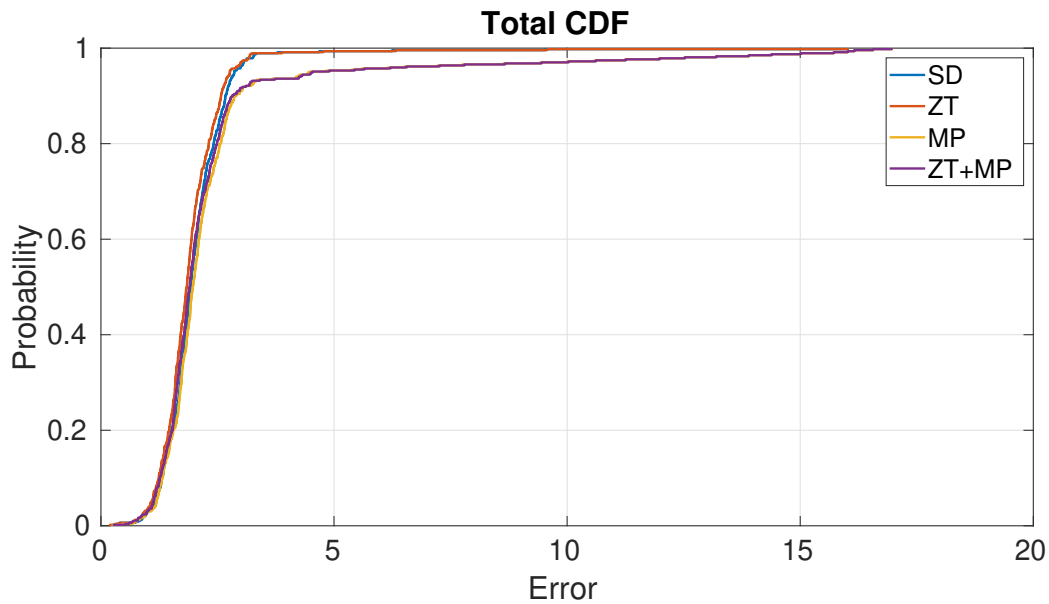
Total CDF

Figure 4: Total Cumulative Distribution (errors are in meters).

A possible explanation for the bad performance of the strategies that tried to estimate the SD multipath errors (MP and ZT+MP) might be associated to the lack of observability/estimability of the m additional states that were included in the EKF [25]. Also, the fact that the SD multipath error correlation times identified in the dynamic test (showed in Table 5) were relatively small may have made them more

Table 1

Mean position errors for the dynamic test.

Error	SD	MP	ZT	ZT+MP
Horizontal [m]	1.19	1.19	1.19	1.19
Vertical [m]	1.44	1.94	1.32	1.87
Total [m]	2.01	2.45	1.92	2.39

Table 2
Horizontal position performance for the dynamic test.

Strategy	Probability (%)		
	<0.5 m	<1.0 m	<1.5 m
SD	8.10	44.14	74.84
MP	8.53	44.99	73.77
ZT	8.10	44.14	74.84
ZT+MP	8.53	44.99	73.77

Table 3
Vertical position performance for the dynamic test.

Strategy	Probability (%)		
	<1.0 m	<2.0 m	<3.0 m
SD	26.65	83.16	98.93
MP	20.68	76.76	94.03
ZT	29.21	87.42	98.94
ZT+MP	23.03	80.81	93.82

Table 4
Total position performance for the dynamic test.

Strategy	Probability (%)		
	<1.0 m	<2.0 m	<3.0 m
SD	2.77	56.72	96.16
MP	2.99	51.81	91.04
ZT	3.41	64.61	97.01
ZT+MP	3.20	58.85	91.68

Table 5
SD multipath error correlation Times and PSDs.

SD error	$\tau_z(s)$	$S_{w_z}(m^2/s)$
$\delta\rho_{M,a}^{p5}$	8,047	0,0095
$\delta\rho_{M,a}^{p6}$	5,806	0,0124
$\delta\rho_{M,a}^{p11}$	11.000	0,0043
$\delta\rho_{M,a}^{p12}$	11.000	0,0041
$\delta\rho_{M,a}^{p24}$	40,803	0,0024
$\delta\rho_{M,a}^{p25}$	10,494	0,0060
$\delta\rho_{M,a}^{p26}$	34,658	0,0053

difficult for the EKF to identify (and estimate) from the pseudorange tracking noise. As analyzed by Hu, Neupane, and Farrell [26], for a moving platform, the receiver moves relative to the reflective surface; therefore, the multipath errors change much more rapidly (i.e., less correlated across time), which makes them easier for the standard SD RT-PPP strategy (that does not try to model the multipath errors as states) to filter out during the vehicle state estimation process. This behavior, and the superior position estimation performance of the SD RT-PPP strategy, have been confirmed in our dynamic test (see Tables 1 to 4 again).

5. Conclusions and Future Work

Accuracy in position estimation is of great interest in many commercial applications. This work investigated the performance of advanced filtering techniques that aimed at mitigating residual pseudorange errors that usually remain after the deployment of SF code-based RT-PPP. The first technique consisted

of estimating the residual zenith wet tropospheric error, which can vary with climate and weather, as an additional state to the associated EKF, via suitable mapping functions. The second technique, in turn, consisted of estimating the SD multipath errors by adding as many states as necessary to the EKF, and determining appropriate correlation times and driven noise PSDs for the 1st-order GM processes proposed to model them. A dynamic test was performed with a focus on complying with position requirements for CVAs in Brazilian territory.

As the results showed, and possibly due to the lack of observability/estimability of the SD multipath error states, as well as to the reduced correlation times identified for the latter, the strategies that attempted to estimate the residual multipath errors, besides increasing the EKF complexity/computational burden, did not bring any additional benefit in terms of position accuracy. The single additional state that was proposed for estimating the residual zenith wet tropospheric error, in turn, proved to be able to improve vertical positioning accuracy in about 12 centimeters, w.r.t. the standard SD RT-PPP approach, which is inline with the predictions by Groves [7]. For future work, one has the performance evaluation of the proposed filtering-based residual error mitigation techniques in the context of integrated Inertial/Global Navigation Satellite Systems (INS/GNSSs), via SF code- and phase-based RT-PPP, specifically aiming to improve observability/estimability constraints.

Acknowledgments

References

[1] G. Lachapelle, GPS observables and error sources for kinematic positioning, Kinematic Systems In Geodesy, Surveying, And Remote Sensing (1991) 17–26.

[2] P. Teunissen, Differential GPS: Concepts and quality control, J Inst. Navig. 10 (1991) 48–60.

[3] J. Farrell, M. Grewal, M. Djodot, M. Barth, Differential GPS with latency compensation for autonomous navigation, in: Proceedings Of the 1996 IEEE Int. Symp. Intell., 1996, pp. 20–24.

[4] F. O. Silva, W. Hu, J. A. Farrell, Real-Time Single-Frequency Precise Point Positioning for Connected Autonomous Vehicles: A Case Study over Brazilian Territory, IFAC Papers-On-line 56 (2023) 5703–5710.

[5] L. Mendoza, A. Meza, J. Aragón Paz, A multi-GNSS, multi-frequency and near real-time ionospheric TEC monitoring system for South America, J Space Weather Res. 17 (2019) 654–661.

[6] I. R. W. Group, IGS IGS state space representation (SSR) format version 1.00., 2020.

[7] P. Groves, Principles of GNSS, Inertial, and Multisensor Integrated Navigation Systems, Artech House, 2013.

[8] L. de Oliveira, I. Ramos, F. Silva, D. de Lima, Comparative analysis between tropospheric models for GNSS positioning in Brazilian territory, in: Proc. ABCM DINAME, 2023.

[9] R. Leandro, M. Santos, R. Langley, UNB neutral atmosphere models: development and performance, in: Proc. of ION NTM, 2006, p. 52.

[10] A. Niell, Global Mapping Functions for the Atmosphere Delay at Radio Wavelengths, J. Geophys. Res. 101 (1996) 3227–3246.

[11] R. Conley, R. Consentino, C. J. Hegarty, E. D. Kaplan, J. L. Leva, M. U. de Haag, K. Van Dyke, Understanding GPS Principles and Applications, Artech House, 2006, pp. 301–378.

[12] J. Farrell, Aided Navigation: GPS with High Rate Sensors, McGraw-Hill, Inc., 2008.

[13] M. S. Braasch, Handbook of Global Navigation Satellite Systems, Springer International Publishing, 2017.

[14] P. Teunissen, O. Montenbruck, Handbook of Global Navigation Satellite Systems, Springer International Publishing, 2017.

[15] T. A. Herring, Modelling atmospheric delays in the analysis of space geodetic data, in: Proc. of Symposium on Refraction of Transatmospheric Signals in Geodesy, 1992, pp. 157–164.

[16] I. A. Ramos, F. O. Silva, L. A. de Oliveira, D. A. de Lima, J. A. Menezes Filho, R. P.and Farrell, On the Performance Degradation of GPS Positioning due to Outdated RT-PPP Products, in: Proc. of Brazilian Symposium on Intelligent Automation, 2023.

[17] Z. Nie, H. Yang, P. Zhou, Y. Gao, Z. Wang, Quality assessment of CNES real-time ionospheric products, GPS Solut. (2019) 1–15.

[18] J. Uwineza, F. Rahman, F. Silva, W. Hu, J. Farrell, Characterizing GNSS Multipath at Different Antenna Mounting Positions on Vehicles, 2019. URL: https://escholarship.org/uc/item/9mj3459s.

[19] R. Brown, P. Hwang, Introduction to random signals and applied Kalman filtering: with MATLAB exercises and solutions, John Wiley and Sons, 1997.

[20] IGS, International gnss service, 2023. URL: https://www.igs.gov/.

[21] L. Mendoza, A. Meza, J. Aragón Paz, Technical note on the multi-GNSS, multi-frequency and near real-time ionospheric TEC monitoring system for South America, 2019.

[22] MAGGIA, Index of /ion/magn/, 2023. URL: https://wilkilen.fcaglp.unlp.edu.ar/ion/magn/.

[23] T. Takasu, N. Nubo, A. Yasuda, Development, Evaluation and Application of RTKLIB: A program library for RTK-GPS, in: Proc. of the GPS/GNSS Symposium, 2007.

[24] SAE, SAE J2945: On-Board System Requirements for V2V Safety Communications. SAE International, 2020.

[25] F. Silva, E. Hemerly, W. C. Leite Filho, On the error state selection for stationary SINS alignment and calibration Kalman filters—Part II: Observability/estimability analysis, sensors 439 (2017).

[26] W. Hu, A. Neupane, J. A. Farrell, Using PPP Information to Implement a Global Real-Time Virtual Network DGNSS Approach, IEEE T. Vehic. Technol. 71 (2022) 10337–10349.